ACS APPLIED MATERIALS & INTERFACES

Research Article

www.acsami.org

Polyelectrolyte Assisted Synthesis and Enhanced Oxygen Reduction Activity of Pt Nanocrystals with Controllable Shape and Size

Lei Du,[†] Sheng Zhang,[†] Guangyu Chen,[†] Geping Yin,[†,‡] Chunyu Du,*[,†] Qiang Tan,[†] Yongrong Sun,[†] Yunteng Qu,[†] and Yunzhi Gao[†]

[†]Institute of Advanced Chemical Power Sources, School of Chemical Engineering and Technology, Harbin Institute of Technology, 92 West Dazhi Street, Harbin 150001, China

[‡]State Key Laboratory of Urban Water Resource and Environment, Harbin Institute of Technology, 73 Huanghe Road, Harbin 150090, China

Supporting Information

ABSTRACT: The shape control of platinum nanocrystals is significant to the enhancement of their catalytic performance in terms of activity and selectivity. However, it still remains a major challenge to prepare Pt nanocrystals with tunable shape and clean surface in an eco-friendly way. This article develops a facile and green strategy to prepare well tuned platinum nanocrystals employing poly(diallyldimethylammonium chloride) (PDDA) as the capping agent, reductant, and stabilizer simultaneously in a facile hydrothermal process. It is identified that the variation of PDDA concentration is crucial to control the growth of crystalline facets, leading to the formation of cubic, truncated cubic, and octahedral Pt nanocrystals with sizes tunable from ca. 17 nm to ca. 50 nm. The resultant Pt nanocrystals exhibit excellent electrocatalytic activity and stability toward the oxygen reduction reaction (ORR) in acidic media compared with those of commercial Pt black and the state-of-the-art Pt/C catalyst. It is proposed that the preferential Pt surface and the decoration of PDDA, which modulates the electronic structures and electrooxidation of Pt nanocrystals, synergistically contribute to the enhanced catalytic performance.

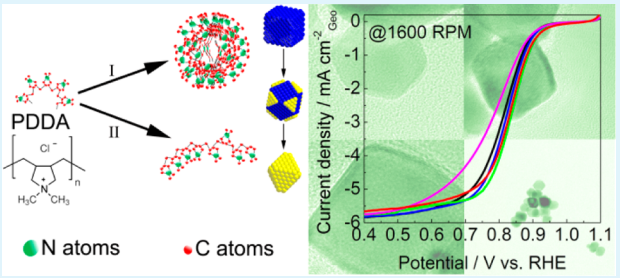

KEYWORDS: *platinum nanocrystals, polyelectrolyte, shape control, electrocatalysts, oxygen reduction reactions*

1. INTRODUCTION

Platinum (Pt) has recently played key roles in a wide variety of applications, such as nitric acid production,[1] electrochemical biosensors,[2] organic synthesis,[3] and electrocatalysis.[4−6] In particular, Pt serves as the most significant eletrocatalyst for proton exchange membrane fuel cells (PEMFCs), which are regarded as the promising candidates to deal with the problems of environmental pollution and energy shortage due to their high efficiency, low emission, low operation temperature, and quick startup.[4,7] The synthesis of Pt electrocatalysts with high activity and long operation life is critical for the development of PEMFCs, which depends not only on the active surface area but also on the nature of exposed lattice planes of Pt.[8−10]

Selective growth of special lattice planes during the crystallization of noble metals has attracted much attention after the first report about the synthesis of Pt nanocrystals (NCs) by EI-Sayed et al.,[11] who obtained polydispersed Pt NCs with different shapes in a hydrogen-reducing way, employing sodium polyacrylate as the capping agent. At present, chemical reduction is the most efficient and convenient strategy to the synthesis of Pt NCs. The key to achieving the controlled shapes of Pt NCs during the chemical reduction is the usage of capping agents to enhance the growth of special facets, which can be (i) macromolecules or polymers, such as cetyltrimethylammonium bromide (CTAB),[12] oleic acid (OA),[13] polyvinylpyrrolidone (PVP),[14−17] poly(acrylic acid) (PAA),[18,19] P123,[20,21] or Brij58,[22] (ii) negatively or positively charged ions, such as Br^-,[15] I^-,[18] NO_3^-,[23] Ag^+,[24,25] Fe^{2+}, and Fe^{3+},[26] (iii) carbonyl compounds, such as $Fe(CO)_5$,[27−29] $Cr(CO)_6$,[30] and $Mn_2(CO)_{10}$,[31,32] and (iv) trace metals such as Co.[33,34] It is noteworthy that, in spite of significant progress in the shape control of Pt NCs, the methods mentioned above are relatively complicated, have a high cost, or are noneco-friendly, mainly due to the employment of noxious organic solvents, delicately selected reductants/stabilizers, and other assistant shape-controlling chemicals. More importantly, the commonly used capping agents, such as PVP, PAA, or halide ions, adsorb on Pt surfaces strongly and block reactants from approaching active sites, thus lowering the electrocatalytic performance of catalysts.

Herein, we employ a polyelectrolyte, poly(diallydimethlammonium chloride) (PDDA), as a "three in one" agent (reductant, stabilizer, and capping agent) to

Received: May 29, 2014
Accepted: July 24, 2014
Published: July 24, 2014

 © 2014 American Chemical Society

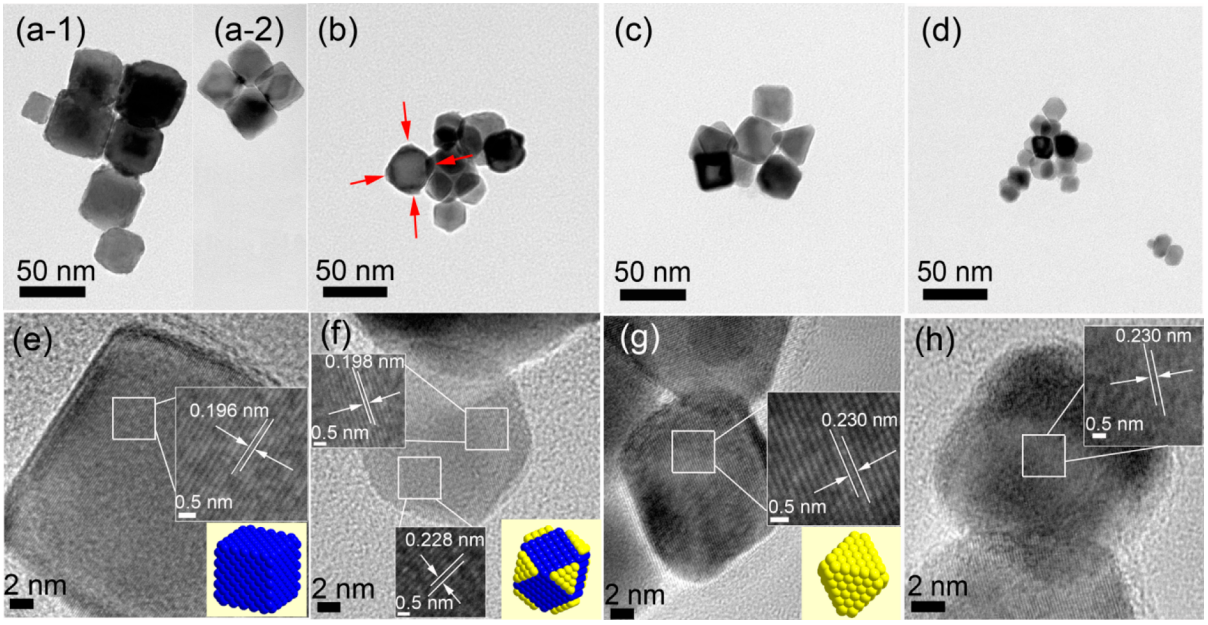

Figure 1. Representative TEM images of (a) ca. 50 nm cubes, (b) ca. 30 nm truncated cubes, (c) ca. 30 nm octahedrons, and (d) ca. 17 nm particles. Representative HRTEM images of (e) cubes, (f) truncated cubes, (g) octahedrons, and (h) particles. The bottom insets are schematic illustrations of corresponding Pt NCs. Blue and yellow spheres represent atoms on Pt (100) and Pt (111) facets, respectively.

synthesize Pt NCs with sizes tunable from ca. 17 nm to ca. 50 nm and shapes controllable from cubes, truncated cubes, to octahedrons for the first time. This synthesis is achieved via a one-pot hydrothermal process by just adjusting the concentration of PDDA in the absence of any other surfactants or agents so that it is simple, of low cost, is up-scalable, and is eco-friendly. Furthermore, the adsorption strength of PDDA is moderate on Pt surfaces, which can be removed from the Pt surfaces more easily.[35−39] More interestingly, different from the commonly used surfactants, it is not necessary to completely remove PDDA from the Pt surfaces,[35−39] because the synergistic contribution of soft PDDA and hard exposed Pt lattice facets leads to even better activity and durability toward the oxygen reduction reaction (ORR). The PDDA decorated Pt octahedrons exhibit about 5-fold higher oxygen reduction kinetics and much better stability than commercial Pt black catalysts.

2. EXPERIMENTAL METHODS

2.1. Materials. PDDA (35 wt %, average MW < 100000), hexachloroplatinic acid ($H_2PtCl_6·6H_2O$), ethanol (CH_3CH_2OH), 5 wt % Nafion solution, and sodium borohydride ($NaBH_4$) were purchased from Sigma-Aldrich and used without any purification. Deionized water (18.2 MΩ, Milli-Q Corp.) was used for all the synthesis of Pt nanocrystals. Pt black was purchased from Johnson-Matthey Corp.

2.2. Preparation of Pt Seeds. Pt seeds, whose average size is around 2.3 nm as revealed by Figure S1 in Supporting Information, were synthesized by a common $NaBH_4$ reduction method using PDDA as a stabilizer. First, H_2PtCl_6 aqueous solution (100 μL, 3.8 mg_{Pt} mL^{-1}) and PDDA were dissolved in some amount of water under vigorous stirring for 10 min. Then, freshly prepared $NaBH_4$ solution was added at once. The reaction lasted for 2 h under stirring, resulting in a complete reduction reaction of H_2PtCl_6.

2.3. Synthesis of Pt Nanocrystals. The Pt nanocrystals were synthesized under hydrothermal conditions in the presence of PDDA. A certain amount of H_2PtCl_6 aqueous solution (10 mL) and several milliliters of water were added into the colloid solution containing the Pt seeds and PDDA, and stirred for ca. 30 min. The concentration of PDDA was 60 mg mL^{-1}, 40 mg mL^{-1}, 30 mg mL^{-1}, and 20 mg mL^{-1}. Then, the obtained pale yellow solution was transferred into a 50 mL Teflon-lined stainless steel autoclave, which was sealed and maintained at 180 °C for 12 h. After naturally cooling down to room temperature, the product was centrifuged at 6000 rpm and washed with water and ethanol several times, and then was freeze-dried into a black powder for further characterization.

2.4. Physical Characterization. The samples were characterized by different analytic techniques. X-ray powder diffraction (XRD) was carried out on a Rigaku D/max-γA X-ray diffractometer with Cu$\kappa\alpha$ radiation (λ = 1.54178 Å). Transmission electron microscopy (TEM) and high resolution TEM (HR-TEM) images were taken with a TecnaiG2F30 transmission electron microscope with an acceleration voltage of 300 kV. X-ray photoelectron spectra (XPS) were recorded on a PHI 5700 ESCA system fitted with $Al_{\kappa\alpha}$ radiation. The energy calibration and deconvolution of XPS peaks were calculated using an XPSpeak software.

2.5. Electrochemical Measurements. The electrochemical tests were carried out in a three-electrode system controlled by a CHI workstation (CHI Instruments, Inc.) with Pt foil and Hg/Hg_2SO_4 (0.68 V versus reversible hydrogen electrode, RHE) as the counter electrode and reference electrode, respectively. The working electrode was prepared by dropping 20 μL of catalyst−water ink (2 $mg_{catalyst}$ mL_{ink}^{-1}) onto the Φ 5 mm glassy-carbon disk electrode (Pt loading is 0.2 mg cm^{-2}). After drying at room temperature, 10 μL of 0.05 wt % Nafion was dropped onto the catalyst surface to form a protective film, and the as-prepared working electrode was dried under argon flow. The working electrode was first activated in N_2-saturated 0.1 mol L^{-1} $HClO_4$ solution by cyclic voltammetry (CV) (0.05−1.2 V at 50 mV s^{-1}) until a steady CV curve was obtained. The oxygen reduction reaction (ORR) was measured using a rotating disk electrode in O_2-saturated 0.1 mol L^{-1} $HClO_4$ with linear sweep voltammetry (LSV) in the potential from 1.1 to 0.4 V at a scan rate of 5 mV s^{-1}. To investigate the durability of catalysts, the working electrode was degraded in N_2-saturated 0.1 mol L^{-1} $HClO_4$ by CV (0.6−1.1 V at 50 mV s^{-1}, 5000 cycles) for ca. 28 h, and the performance was tested before and after degradation via the methods mentioned above. More characterization details are provided in Supporting Information. All of the tests were conducted at 25 °C with a thermostatic water bath. All potentials mentioned were reported with respect to RHE.

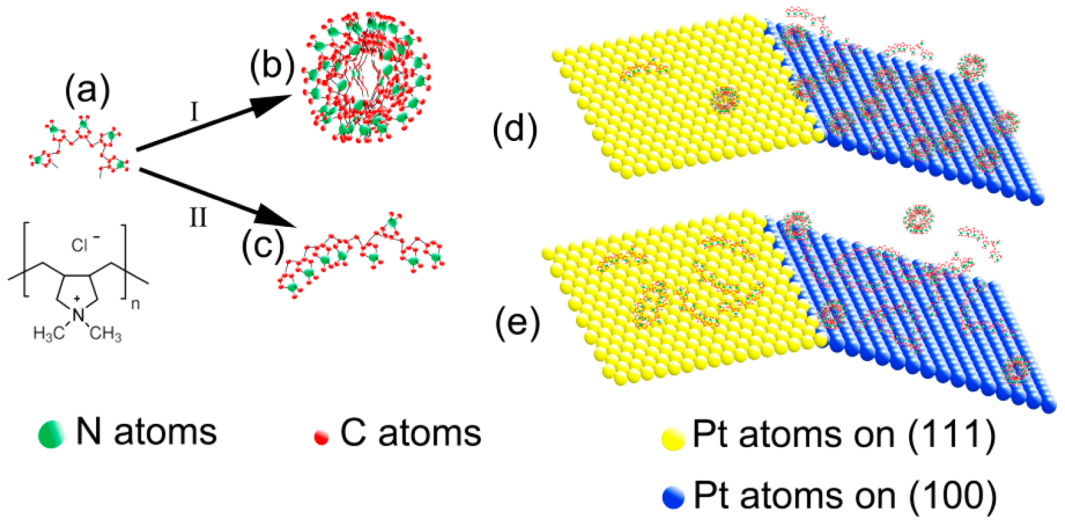

Figure 2. Schematic illustrations of (a) PDDA molecular chains and the structural formula of a PDDA monomer; (b) micelle structure at high PDDA concentrations; (c) twisty long-chain at low PDDA concentrations; adsorbed (d) micelles with exposed amino groups; and (e) twisty long-chain PDDA on Pt facets.

3. RESULTS

Generally, polyhedral Pt NCs are enclosed by (111) and/or (100) facets, which govern the morphology of Pt NCs, such as cubes, octahedrons, or icosahedrons.[8−10,40] In this article, the morphology of Pt NCs is controlled by the PDDA concentration during the hydrothermal process. TEM is employed to follow the morphology evolution of the Pt NCs prepared by different PDDA concentrations.[41] TEM images in Figure 1a−d show the morphology of Pt NCs changed from cubes to spherical particles via truncated cubes and octahedrons with the decrease in PDDA concentration. When the PDDA concentration is 60 mg mL^{-1}, cubic Pt NCs are formed. As the PDDA concentration is reduced to 40 mg mL^{-1} and 30 mg mL^{-1}, truncated cubic and octahedral Pt NCs are produced in sequence. By the further reduction of the PDDA concentration to 20 mg mL^{-1}, uniform spherical Pt nanoparticles are obtained. In addition to morphology, PDDA can also modulate the size of Pt NCs. As the PDDA concentration decreases, the size of Pt NCs, which is uniform, decreases from 50 to 17 nm. The shape and size variation clearly demonstrates that PDDA can serve as an efficient capping agent and stabilizer to control the morphology of Pt NCs. It is noteworthy that PDDA can serve not only as a capping agent and stabilizer but also as a reductant to synthesize the Pt NCs. Without the addition of PDDA, only the PtO_2 product is obtained as revealed by XRD and TEM (Figures S2 and S3 in Supporting Information), indicating that $PtCl_6^{2-}$ could not be reduced without PDDA. In order to get accurate lattice fringes and analyze arrangements of facets, HR-TEM of the Pt NCs is employed to determine the distance between two columns of atoms. Figure 1e and g shows lattice fringe spacings of 0.196 and 0.230 nm, which can be assigned to the (100) facet of Pt cubes and the (111) facet of Pt octahedrons, respectively. Figure 1f shows lattice fringe spacings of 0.198 and 0.228 nm, which are assigned to the (100) and (111) facets of truncated cubic Pt NCs, respectively. Figure 1h presents a lattice fringe spacing of 0.230 nm, which is assigned to (111) facet of Pt particles. Moreover, as indicated by the red arrows in Figure 1b, obvious chamferings confirm the morphology of truncated cubic Pt NCs, an evolution of cubes. All of these results imply that along with the PDDA concentration decreasing, the preferential facet transforms from Pt (100) to Pt (111).

A proposed mechanism for controlling the morphology of Pt NCs by PDDA is illustrated in Figure 2. PDDA, a long-chain polyelectrolyte that does not change the existing form of the Pt precursor as revealed by the UV−vis spectra (Figure S4 in Supporting Information), includes hydrophilic groups (positively charged amino parts) and hydrophobic groups (hydrocarbyl parts) (Figure 2a). The polymers with hydrophilic and hydrophobic groups, such as the poly(styrene)-*b*-poly(acrylic acid) and sodium dodecyl sulfate, can form micelles,[42,43] the shape and size of which depend on the concentration of polymers.[44,45] On the basis of these results, when the PDDA concentration is high, positively charged hydrophilic groups move outward spontaneously to form a spherical-like micelle structure with large amounts of amino groups exposed (Route I, Figure 2b). In the case of low PDDA concentration, most PDDA chains turn to be a twisty structure without particular orientation (Route II, Figure 2c). It has been reported that amino-ligands are preferentially adsorbed by Pt (100) facets.[28,29] Therefore, lots of spherical-like structures with copious amino groups exposed will block the growth of Pt (100) facets and lead to the formation of more (100) facets in the final Pt NCs, such as Pt cubes in Figure 1a, following the Bravais law (Figure 2d).[46] In contrast, twisty structures are not strongly adsorbed by Pt (100) facets because the disordered hydrocarbyl chains enclose amino groups (Figure 2e). Thus, the final Pt NCs are made up of most Pt (111) facets due to the minimum energy principle,[41] leading to the Pt octahedrons in Figure 1c. When the PDDA concentration is moderate, a mixture of Pt (111) and (100) facets appears, and truncated cubic Pt NCs are formed (Figure 1b). In a very low concentration, PDDA loses the function of a capping agent and acts only as a stabilizer and reductant, resulting in the formation of spherical Pt NCs (Figure 1d). Actually, our method using PDDA as a "three in one" agent can control the morphology of not only Pt but also Pt-based alloy NCs (Figure S5 in Supporting Information).

To further probe the crystalline facets of the prepared Pt NCs, CVs of Pt cubes, truncated cubes, octahedrons, and spherical particles were carried out in 0.1 mol L^{-1} perchloric

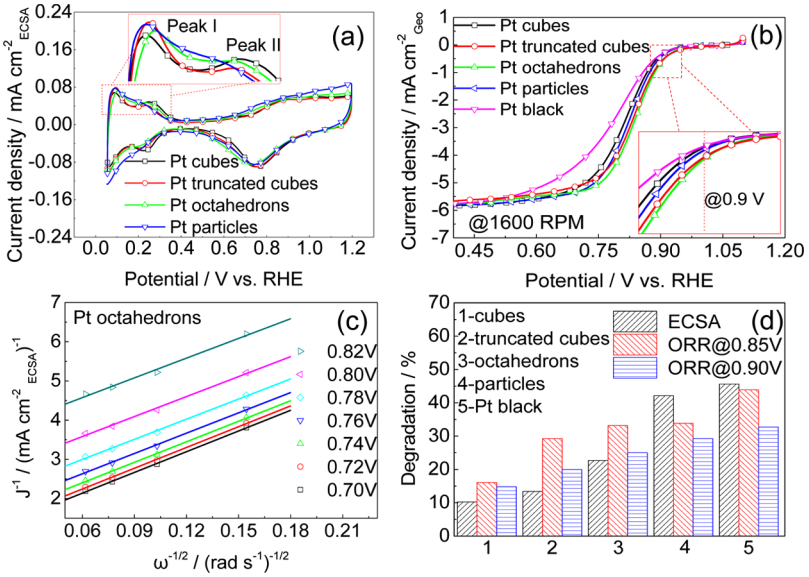

Figure 3. (a) Cyclic voltammograms of Pt NCs in nitrogen-saturated 0.1 mol L^{-1} $HClO_4$ solution at a scan rate of 50 mV s^{-1}. (b) Linear sweep voltammograms of Pt NCs and commercial Pt black in oxygen-saturated 0.1 mol L^{-1} $HClO_4$ solution at 1600 rpm and a scan rate of 5 mV s^{-1} (the inset shows details of LSVs at 0.9 ± 0.05 V). (c) Koutecky–Levich curves for Pt octahedrons at 0.7 V–0.82 V. (d) Degradation percentages of ECSA and ORR kinetic activity of Pt NCs and Pt black after the CV durability test for 28 h.

Table 1. Kinetic Activity of Pt NCs and Commercial Pt Black for the Oxygen Reduction Reaction

	kinetic current density/I_k			
	ORR @ 0.85 V [mA mg^{-1}_{Pt}]^a	ORR @ 0.85 V [mA cm^{-2}_{ECSA}]^b	ORR @ 0.90 V [mA mg^{-1}_{Pt}]^a	ORR @ 0.90 V [mA cm^{-2}_{ECSA}]^b
Pt cubes	50.01	1.37	10.00	0.27
Pt truncated cubes	80.00	1.95	16.25	0.40
Pt octahedrons	132.50	2.23	22.61	0.38
Pt nanoparticles	62.50	0.65	12.25	0.13
Pt black	35.00	0.41	9.25	0.11

^{a}All Pt catalysts are in the same loading (0.2 mg cm^{-2}) on the glassy-carbon electrode during tests. ^{b}ECSA is a calculated value based on profiles of hydrogen desorption in cyclic voltammograms; all ORR kinetic activities are calculated according to the Koutecky–Levich equation.

acid ($HClO_4$) solution (Figure 3a). The two voltammetric peaks (Peak I and Peak II) between 0.05 and 0.3 V are profiles of hydrogen adsorption and desorption on the surfaces of Pt electrodes, which correspond to different crystalline facets and are also used to evaluate the electrochemical active surface area (ECSA) of Pt NCs.[47] It is established that Peak II is correlated with the Pt (100) facets, and thus, the intensity of Peak II reflects the relative amount of the Pt (100) facets in the Pt NCs.[29,48] Apparently, the intensity of Peak II for Pt cubes (high PDDA concentration) is higher than that of other Pt NCs (lower PDDA concentrations). As the PDDA concentration decreases, the intensity of Peak II decreases as well. This observation indicates that higher PDDA concentrations induce the formation of more Pt (100) facets, which is in accordance with the TEM images in Figure 1. The parallel CV tests of the Pt NCs in sulfuric acid solution (Figure S6 in Supporting Information) also support this inference.[49]

Figure 3b shows linear sweep voltammograms (LSVs) of Pt cubes, truncated cubes, octahedrons, spherical particles, and Pt black toward the ORR, which are carried out in oxygen-saturated 0.1 mol L^{-1} $HClO_4$ solution using the rotating disk electrode at 1600 rpm. It is revealed that the onset potential sequence for the ORR is Pt octahedrons > truncated cubes > particles > cubes > Pt black. To investigate the intrinsic ORR activities, the kinetic current densities at 0.9 and 0.85 V are calculated and collected in Table 1 by using the Koutecky–Levich equation:

$$\frac{1}{I} = \frac{1}{I_k} + \frac{1}{I_d} \quad (1)$$

$$I_d = 0.62nFAD^{2/3}\nu^{-1/6}c_0\omega^{1/2} \quad (2)$$

where I and I_k are the experimental and kinetic current densities, n the transferred electron number, F the Faraday constant (96485 C mol^{-1}), A the geometric electrode area, D the oxygen diffusivity (1.93×10^{-5} cm^2 s^{-1}),[50] ν the solution viscosity (1.009×10^{-2} cm^2 s^{-1}),[50] c_O the concentration of dissolved O_2 in solution (1.26×10^{-6} mol cm^{-3}),[51] and ω the angular velocity of the disk. All of the Pt NCs show higher ORR activities than commercial Pt black. In particular, the Pt octahedrons (ca. 2.23 mA cm^{-2}) exhibit ca. 5.4 times higher specific activity than the commercial Pt black (ca. 0.41 mA cm^{-2}) at 0.85 V, which also present higher specific activity than the state-of-the-art Pt/C catalyst.[13] The mass activity of Pt octahedrons is 132.50 mA mg^{-1}_{Pt} at 0.85 V, which is also 3.8 times higher than that of Pt black (35 mA mg^{-1}_{Pt}). As mentioned above, the Pt octahedrons have the most (111) facets, which are more active for the ORR than other facets in the $HClO_4$ solutions.[48] Therefore, the Pt octahedrons are the most active for the ORR among all of the Pt NCs. On the basis of the Koutecky–Levich equation,[52,53] the transferred electron

number during the ORR is also calculated to be 3.8 and 3.1 for Pt octahedrons (Figure 3c) and Pt black (Figure S7 in Supporting Information), respectively. This result means that oxygen is mainly reduced via a four-electron process on Pt octahedrons, whereas Pt black presents a more two-electron process, which is not favored for the ORR.[54]

The durability of the Pt NCs is studied by the accelerated aging test in the potential range of the formation and reduction of Pt oxides (0.6−1.1 V).[47] Figure 3d shows the degradation of ECSA and kinetic ORR activity of the Pt NCs and Pt black in the durability tests according to the CV results (Figure S8 and Table S1 in Supporting Information). All of the Pt NCs present higher stability than Pt black. Especially, Pt cubes, which are prepared by the highest PDDA concentration, exhibit the best stability. This result implies that the absorbed PDDA can protect Pt NCs from electrooxidation and dissolution, thus leading to higher durability since the electrooxidation and dissolution are regarded as the dominating reason for the degradation of Pt ORR catalysts.[35] Actually, the regulating of electronic properties of Pt by PDDA also improves the stability of the Pt NCs, which will be discussed below.

XPS is employed to detect the electronic interaction between Pt and PDDA. The full XPS spectra (Figure S9 in Supporting Information) confirm the presence of Pt and N elements, which indicates that PDDA is definitely absorbed on the surfaces of Pt NCs. Figure 4a gives a relatively obvious peak of N 1s in Pt

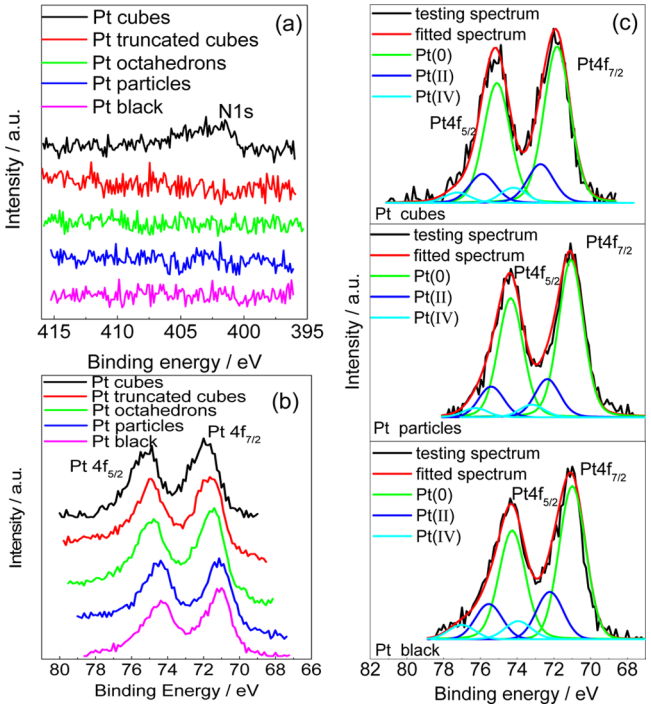

Figure 4. (a) N 1s region, (b) Pt 4f region, and (c) deconvolutions of XPS spectra of Pt NCs and commercial Pt black.

cubes, which comes from PDDA and is due to the highest PDDA absorption during the synthesis. Figure 4b shows the detailed Pt 4f spectra, from which the PDDA concentration apparently affects the binding energy of Pt. The Pt cubes prepared by the highest PDDA concentration exhibit the most positive shift of the binding energy. This shift is most likely due to the electron transfer from Pt to N,[55] which facilitates the ORR process,[56,57] decreases the oxidation degree of Pt,[47] and enhances the durability.[35] From the deconvoluted XPS results (Figure 4c), the Pt NCs contain more Pt (0) and less Pt (II) or Pt (IV) (Table S2 in Supporting Information), which should be due to the electronic effects and reducibility of PDDA.

4. CONCLUSIONS

In summary, we develop a general strategy to prepare Pt nanocrystals with specific facets by using PDDA as a "three in one" agent in a facile hydrothermal process. The key to this synthesis is the morphology transformation of PDDA at different concentrations, which presents a spherical-like micelle structure or twisty long-chain structure at high or low concentrations, respectively. By modulating the PDDA concentration, well-defined cubic, truncated cubic, and octahedral Pt nanocrystals can be obtained with sizes tunable from ca. 17 nm to ca. 50 nm. These Pt nanocrystals show higher activity and stability toward the oxygen reduction reaction, which can be attributed to the synergistic contribution of the optimized Pt facets and the decorative PDDA that can mitigate the electrooxidation and dissolution and modulate the electronic structures of Pt nanocrystals. Our developed method can be extended to other metal or alloy nanocrystals with high electrochemical performance.

■ ASSOCIATED CONTENT

Supporting Information

XRD pattern and TEM image of the samples without PDDA; UV−vis spectra of the precursors; CV curves, Koutecky−Levich plots, and durability testing curves; wide range XPS spectra of Pt nanocrystals and commercial Pt black; and shapes of PDDA-tuned PtAu nanocrystals. This material is available free of charge via the Internet at http://pubs.acs.org.

■ AUTHOR INFORMATION

Corresponding Author

*Phone: 86-451-86403961. E-mail: cydu@hit.edu.cn

Notes

The authors declare no competing financial interest.

■ ACKNOWLEDGMENTS

This work is supported by National Natural Science Foundation of China (Grant Nos. 21276058, 21376057, and 21106024).

■ REFERENCES

(1) Perez-Ramirez, J.; Kapteijn, F.; Schoffel, K.; Moulijn, J. A. Formation and Control of N_2O in Nitric Acid Production: Where Do We Stand Today? *Appl. Catal., B* **2003**, *44*, 117−151.

(2) Niu, X.; Lan, M.; Zhao, H.; Chen, C. Well-Dispersed Pt Cubes on Porous Cu Foam: High-Performance Catalysts for the Electrochemical Oxidation of Glucose in Neutral Media. *Chem.—Eur. J.* **2013**, *19*, 9534−9541.

(3) Alayoglu, S.; Aliaga, C.; Sprung, C.; Somorjai, G. A. Size and Shape Dependence on Pt Nanoparticles for the Methylcyclopentane/Hydrogen Ring Opening/Ring Enlargement Reaction. *Catal. Lett.* **2011**, *141*, 914−924.

(4) Kloke, A.; Stetten, F. V.; Zengerle, R.; Kerzenmacher, S. Strategies for the Fabrication of Porous Platinum Electrodes. *Adv. Mater.* **2011**, *23*, 4976−5008.

(5) Yamauchi, Y. Field-Induced Alignment Controls of One-Dimensional Mesochannels in Mesoporous Materials. *J. Ceram. Soc. Jpn.* **2013**, *121*, 831−840.

(6) Li, C.; Sato, T.; Yamauchi, Y. Electrochemical Synthesis of One-Dimensional Mesoporous Pt Nanorods Using the Assembly of

Surfactant Micelles in Confined Space. *Angew. Chem., Int. Ed.* **2013**, *52*, 8050−8053.
(7) Chu, S.; Majumdar, A. Opportunities and Challenges for A Sustainable Energy Future. *Nature* **2012**, *488*, 294−303.
(8) Chen, M.; Wu, B.; Yang, J.; Zheng, N. Small Adsorbate-Assisted Shape Control of Pd and Pt Nanocrystals. *Adv. Mater.* **2012**, *24*, 862−879.
(9) Sau, T. K.; Rogach, A. L. Nonspherical Noble Metal Nanoparticles: Colloid-Chemical Synthesis and Morphology Control. *Adv. Mater.* **2010**, *22*, 1781−1804.
(10) Tao, A. R.; Habas, S.; Yang, P. Shape Control of Colloidal Metal Nanocrystals. *Small* **2008**, *4*, 310−325.
(11) Ahmadi, T. S.; Wang, Z. L.; Green, T. C.; Henglein, A.; El-Sayed, M. A. Shape-Controlled Synthesis of Colloidal Platinum Nanoparticles. *Science* **1996**, *272*, 1924−1926.
(12) Yang, W.; Wang, X.; Yang, F.; Yang, C.; Yang, X. Carbon Nanotubes Decorated with Pt Nanocubes by a Noncovalent Functionalization Method and Their Role in Oxygen Reduction. *Adv. Mater.* **2008**, *20*, 2579−2587.
(13) Zhou, W.; Wu, J.; Yang, H. Highly Uniform Platinum Icosahedra Made by Hot Injection-Assisted GRAILS Method. *Nano Lett.* **2013**, *13*, 2870−2874.
(14) Dahal, N.; Garcia, S.; Zhou, J.; Humphrey, S. M. Beneficial Effects of Microwave-Assisted Heating Versus Conventional Heating in Noble Metal Nanoparticle Synthesis. *ACS Nano* **2012**, *6*, 9433−9446.
(15) Tsung, C. K.; Kuhn, J. N.; Huang, W.; Aliaga, C.; Hung, L. I.; Somorjai, G. A.; Yang, P. Sub-10 nm Platinum Nanocrystals with Size and Shape Control: Catalytic Study for Ethylene and Pyrrole Hydrogenation. *J. Am. Chem. Soc.* **2009**, *131*, 5816−5822.
(16) Song, H.; Kim, F.; Connor, S.; Somorjai, G. A.; Yang, P. Pt Nanocrystals: Shape Control and Langmuir-Blodgett Monolayer Formation. *J. Phys. Chem. B* **2005**, *109*, 188−193.
(17) Narayanan, R.; El-Sayed, M. A. Effect of Nanocatalysis in Colloidal Solution on the Tetrahedral and Cubic Nanoparticle Shape: Electron-Transfer Reaction Catalyzed by Platinum Nanoparticles. *J. Phys. Chem. B* **2004**, *108*, 5726−5733.
(18) Miyake, M.; Miyabayashi, K. Shape and Size Controlled Pt Nanocrystals as Novel Model Catalysts. *Catal. Surv. Asia* **2011**, *16*, 1−13.
(19) Cao, M.; Miyabayashi, K.; Shen, Z.; Ebitani, K.; Miyake, M. Olefin Hydrogenation Catalysis of Platinum Nanocrystals with Different Shapes. *J. Nanopart. Res.* **2011**, *13*, 5147−5156.
(20) Li, C.; Yamauchi, Y. Facile Solution Synthesis of Ag@ Pt Core−Shell Nanoparticles with Dendritic Pt Shells. *Phys. Chem. Chem. Phys.* **2013**, *15*, 3490−3496.
(21) Wang, L.; Yamauchi, Y. Block Copolymer Mediated Synthesis of Dendritic Platinum Nanoparticles. *J. Am. Chem. Soc.* **2009**, *131*, 9152−9153.
(22) Li, C.; Imura, M.; Yamauchi, Y. A Universal Approach to the Preparation of Colloidal Mesoporous Platinum Nanoparticles with Controlled Particle Sizes in a Wide Range from 20 to 200 nm. *Phys. Chem. Chem. Phys.* **2014**, *16*, 8787−8790.
(23) Herricks, T.; Chen, J.; Xia, Y. Polyol Synthesis of Platinum Nanoparticles: Control of Morphology with Sodium Nitrate. *Nano Lett.* **2004**, *4*, 2367−2371.
(24) Long, N. V.; Chien, N. D.; Hayakawa, T.; Matsubara, T.; Ohtaki, M.; Nogami, M. Sharp Cubic and Octahedral Morphologies of Poly(Vinylpyrrolidone)-Stabilised Platinum Nanoparticles by Polyol Method in Ethylene Glycol: Their Nucleation, Growth and Formation Mechanisms. *J. Exp. Nanosci.* **2012**, *7*, 133−149.
(25) Grass, M. E.; Yue, Y.; Habas, S. E.; Rioux, R. M.; Teall, C. I.; Yang, P.; Somorjai, G. A. Silver Ion Mediated Shape Control of Platinum Nanoparticles: Removal of Silver by Selective Etching Leads to Increased Catalytic Activity. *J. Phys. Chem. C* **2008**, *112*, 4797−4804.
(26) Chen, J.; Herricks, T.; Xia, Y. Polyol Synthesis of Platinum Nanostructures: Control of Morphology through the Manipulation of Reduction Kinetics. *Angew. Chem.* **2005**, *117*, 2645−2648.
(27) Kim, C.; Kim, S. S.; Yang, S.; Han, J. W.; Lee, H. In Situ Shaping of Pt Nanoparticles Directly Overgrown on Carbon Supports. *Chem. Commun.* **2012**, *48*, 6396−6398.
(28) Wang, C.; Daimon, H.; Lee, Y.; Kim, J.; Sun, S. Synthesis of Monodisperse Pt Nanocubes and Their Enhanced Catalysis for Oxygen Reduction. *J. Am. Chem. Soc.* **2007**, *129*, 6974−6975.
(29) Wang, C.; Daimon, H.; Onodera, T.; Koda, T.; Sun, S. A General Approach to the Size- and Shape-Controlled Synthesis of Platinum Nanoparticles and Their Catalytic Reduction of Oxygen. *Angew. Chem., Int. Ed.* **2008**, *47*, 3588−3591.
(30) Loukrakpam, R.; Chang, P.; Luo, J.; Fang, B.; Mott, D.; Bae, I. T.; Naslund, H. R.; Engelhard, M. H.; Zhong, C. J. Chromium-Assisted Synthesis of Platinum Nanocube Electrocatalysts. *Chem. Commun.* **2010**, *46*, 7184−7186.
(31) Kang, Y.; Li, M.; Cai, Y.; Cargnello, M.; Diaz, R. E.; Gordon, T. R.; Wieder, N. L.; Adzic, R. R.; Gorte, R. J.; Stach, E. A.; Murray, C. B. Heterogeneous Catalysts Need Not Be so "Heterogeneous": Monodisperse Pt Nanocrystals by Combining Shape-Controlled Synthesis and Purification by Colloidal Recrystallization. *J. Am. Chem. Soc.* **2013**, *135*, 2741−2747.
(32) Kang, Y.; Pyo, J. B.; Ye, X.; Diaz, R. E.; Gordon, T. R.; Stach, E. A.; Murray, C. B. Shape-Controlled Synthesis of Pt Nanocrystals: The Role of Metal Carbonyls. *ACS Nano* **2013**, *7*, 645−653.
(33) Lim, S. I.; Ojea-Jimenez, I.; Varon, M.; Casals, E.; Arbiol, J.; Puntes, V. Synthesis of Platinum Cubes, Polypods, Cuboctahedrons, and Raspberries Assisted by Cobalt Nanocrystals. *Nano Lett.* **2010**, *10*, 964−973.
(34) Lim, S. I.; Varon, M.; Ojea-Jimenez, I.; Arbiol, J.; Puntes, V. Exploring the Limitations of the Use of Competing Reducers to Control the Morphology and Composition of Pt and PtCo Nanocrystals. *Chem. Mater.* **2010**, *22*, 4495−4504.
(35) Zhang, S.; Shao, Y.; Yin, G.; Lin, Y. Stabilization of Platinum Nanoparticle Electrocatalysts for Oxygen Reduction Using Poly(diallyldimethylammonium chloride). *J. Mater. Chem.* **2009**, *19*, 7995−8001.
(36) Zhang, S.; Shao, Y.; Liao, H. G.; Liu, J.; Aksay, I. A.; Yin, G.; Lin, Y. Graphene Decorated with PtAu Alloy Nanoparticles: Facile Synthesis and Promising Application for Formic Acid Oxidation. *Chem. Mater.* **2011**, *23*, 1079−1081.
(37) Zhang, S.; Shao, Y.; Yin, G.; Lin, Y. Electrostatic Self-Assembly of A Pt-around-Au Nanocomposite with High Activity towards Formic Acid Oxidation. *Angew. Chem., Int. Ed.* **2010**, *49*, 2211−2214.
(38) Zhang, S.; Shao, Y.; Liao, H.; Engelhard, M. H.; Yin, G.; Lin, Y. Polyelectrolyte-Induced Reduction of Exfoliated Graphite Oxide: A Facile Route to Synthesis of Soluble Graphene Nanosheets. *ACS Nano* **2011**, *5*, 1785−1791.
(39) Chen, H.; Wang, Y.; Dong, S. An Effective Hydrothermal Route for the Synthesis of Multiple PDDA-Protected Noble-Metal Nanostructures. *Inorg. Chem.* **2007**, *46*, 10587−10593.
(40) Chen, J.; Lim, B.; Lee, E. P.; Xia, Y. Shape-Controlled Synthesis of Platinum Nanocrystals for Catalytic and Electrocatalytic Applications. *Nano Today* **2009**, *4*, 81−95.
(41) Wang, Z. L. Transmission Electron Microscopy of Shape-Controlled Nanocrystals and Their Assemblies. *J. Phys. Chem. B* **2000**, *104*, 1153−1175.
(42) Ma, N.; Wang, Y.; Wang, B.; Wang, Z.; Zhang, X. Interaction between Block Copolymer Micelles and Azobenzene-Containing Surfactants: From Coassembly in Water to Layer-by-Layer Assembly at the Interface. *Langmuir* **2007**, *23*, 2874−2878.
(43) Manna, U.; Patil, S. Dual Drug Delivery Microcapsules via Layer-by-Layer Self-Assembly. *Langmuir* **2009**, *25*, 10515−10522.
(44) Kayitmazer, A. B.; Shaw, D.; Dubin, P. L. Role of Polyelectrolyte Persistence Length in the Binding of Oppositely Charged Micelles, Dendrimers, and Protein to Chitosan and Poly(dimethyldiallyammonium chloride). *Macromolecules* **2005**, *38*, 5198−5204.
(45) Pavlukhina, S.; Sukhishvili, S. Polymer Assemblies for Controlled Delivery of Bioactive Molecules from Surfaces. *Adv. Drug Delivery Rev.* **2011**, *63*, 822−836.

(46) Donnay, J. D. H.; Harker, D. A New Law of Crystal Morphology Extending the Law of Bravais. *Am. Mineral.* **1937**, *22*, 446−467.
(47) Zhang, J.; Sasaki, K.; Sutter, E.; Adzic, R. R. Stabilization of Platinum Oxygen-Reduction Electrocatalysts Using Gold Clusters. *Science* **2007**, *315*, 220−222.
(48) Markovic, N.; Gasteiger, H.; Ross, P. N. Kinetics of Oxygen Reduction on Pt(hkl) Electrodes: Implications for the Crystallite Size Effect with Supported Pt Electrocatalysts. *J. Electrochem. Soc.* **1997**, *144*, 1591−1597.
(49) Solla-Gullon, J.; Vidal-Iglesias, F. J.; Rodriguez, P.; Herrero, E.; Feliu, J. M.; Clavilier, J.; Aldaz, A. In Situ Surface Characterization of Preferentially Oriented Platinum Nanoparticles by Using Electrochemical Structure Sensitive Adsorption Reactions. *J. Phys. Chem. B* **2004**, *108*, 13573−13575.
(50) Markovic, N. M.; Gasteiger, H. A.; Grgur, B. N.; Ross, P. N. Oxygen Reduction Reaction on Pt(111): Effects of Bromide. *J. Electroanal. Chem.* **1999**, *467*, 157−163.
(51) Hong, J. W.; Kang, S. W.; Choi, B. S.; Kim, D.; Lee, S. B.; Han, S. W. Controlled Synthesis of Pd-Pt Alloy Hollow Nanostructures with Enhanced Catalytic Activities for Oxygen Reduction. *ACS Nano* **2012**, *6*, 2410−2419.
(52) Treimer, S.; Tang, A.; Johnson, D. C. A Consideration of the Application of Koutecký-Levich Plots in the Diagnoses of Charge-Transfer Mechanisms at Rotated Disk Electrodes. *Electroanalysis* **2002**, *14*, 165−171.
(53) Zhang, J.; Mo, Y.; Vukmirovic, M. B.; Klie, R.; Sasaki, K.; Adzic, R. R. Platinum Monolayer Electrocatalysts for O_2 Reduction: Pt Monolayer on Pd (111) and on Carbon-Supported Pd Nanoparticles. *J. Phys. Chem. B* **2004**, *108*, 10955−10964.
(54) Wu, J. B.; Yang, H. Platinum-Based Oxygen Reduction Electrocatalysts. *Acc. Chem. Res.* **2013**, *46*, 1848−1857.
(55) Murgai, V.; Raaen, S.; Strongin, M.; Garrett, R. F. Core-Level and Valence-Band Photoemission Study of Granular Platinum Films. *Phys. Rev. B: Condens. Matter Mater. Phys.* **1986**, *33*, 4345−4348.
(56) Tian, Z. Q.; Jiang, S. P.; Liu, Z. C.; Li, L. Polyelectrolyte-Stabilized Pt Nanoparticles as New Electrocatalysts for Low Temperature Fuel Cells. *Electrochem. Commun.* **2007**, *9*, 1613−1618.
(57) Wang, S.; Yang, F.; Jiang, S. P.; Chen, S.; Wang, X. Tuning the Electrocatalytic Activity of Pt Nanoparticles on Carbon Nanotubes via Surface Functionalization. *Electrochem. Commun.* **2010**, *12*, 1646−1649.